Chapter 3. Design Polygon Shaped Antennas for Hyperthermia Applications at MICS Band

This chapter is divided into two parts. In the first part, a hexagon-shaped patch antenna and in the second part a pentagon patch antenna for hyperthermia applications at 434 MHz are presented.

3.1. SAR Analysis of Hexagonal-Shaped Slot Loaded Patch Antenna for Hyperthermia Applications at 434 MHz

3.1.1. Introduction

Despite the increased interest in cancer treatment in recent years, there have been only a few research articles in the past on the microstrip patch antenna with a planar phantom. The novelty of this proposed antenna lies in obtaining the ISM band of 434 MHz with a comparable value of SAR. In this chapter, a hexagonal-shaped microstrip patch antenna was simulated, fabricated, and measured to study the SAR performance which will extend further for Hyperthermia applications.

3.1.2. Antenna Design

In this section, a hexagonal microstrip patch is designed to cover the ISM band of 434 MHz using FR-4 substrate (dielectric constant ε_r = 4.4, thickness h = 1.6 mm, and loss tangent tanδ = 0.02). The hexagonal patch of major radius R1=30 mm, a concentric annular ring of inner major radius R2= 40mm, and outer major radius R3= 50mm, on the dielectric substrate. Dimensions of the hexagon patch were given from a set of equations (3.1-3.3) [107]. The proposed antenna geometry starts with a classical hexagon shape which manifests the resonant frequency deep higher beyond the MICS band. After covering this hexagonal patch with a hexagonal annular-shaped ring resonant frequency lies near 500 MHz with poorly matched. Now, in antenna-3 ground side is covered by two rectangular orthogonal slots of different lengths and have the same width (w) and the resonance frequency is shifted to the lower frequency band at nearly 400 MHz. Finally, the ground slot by combined with a square slot of side (a) positioned behind the centre of the patch which results in the impedance matching point at 434 MHz because of the lesser current path from the previous one. The evaluation of the proposed antenna configuration is illustrated in Figure 3.1 and the results associated with each stage are given in Figure 3.2. Dimensions of the slots were given from a set of equations(4-9) [108, 109]. Slots in the ground plane act like a load that can be used to bring the input impedance point closer to the characteristic impedance when added to the antenna. The geometrical parameters of the proposed structure are shown in Table 3.1. A 50-ohm coaxial feed is applied inside the annular ring with an inner to power-fed the antenna. Single-layered TEL (tissue equivalent liquid) planar phantom has been taken into consideration throughout the procedure.

The resonant frequency for the lowest order mode is given as [107],

$$\beta S = 2.01 \tag{3.1}$$

The equivalent radius (Req) of a hexagon patch is given as [107],

$$\pi R_{eq}^2 = \frac{3\sqrt{3}S^2}{2} \tag{3.2}$$

The frequency can be determined using the equation provided below after obtaining the radius,

Thus,

$$f_r = \frac{K_{nm}c}{2\pi(R_{eq})\sqrt{\varepsilon_r}} \tag{3.3}$$

Where β is the phase constant and is equal to 2π/λ, and λ is inversionally proportional to the frequency , S is the side of the hexagon, K_{nm} is the m^{th} zero of the derivative of the Bessel function of order n, and c is the velocity of light in free space.

Mathematical calculation for the slot on the ground plane [108, 109],

When a slot is embedded in a patch, having dimension ($L_s \times W_s$), it can be analyzed by using the duality relationship between the dipole and slot [109].

The radiation resistance of the slot is given as,

$$R_r = \frac{\eta cos^2\alpha}{2\pi}\int_0^{\pi}\left[\frac{\cos\frac{k^2 cos\theta}{2} - \cos\frac{kL_s}{2}}{sin\theta}\right]d\theta \tag{3.4}$$

The total input impedance of the slot as,

$$Z_{slot} = \frac{\eta^2}{4Z_{cy}} \tag{3.5}$$

Where Z_{cy} is given as

$$Z_{cy} = R_r(kL_s)\text{-j}\left\{120(ln\left(\frac{L_s}{W_s}\right) - 1)cot\frac{kL_s}{2} - X_r(kL_s)\right\} \tag{3.6}$$

Where R_r is the real part and equivalent to the radiation resistance of the slot and X_r is the input reactance of the slot and given as,

$$X_r = 30cos^2\alpha\{2S_i(kL_s) + cos(kL_s)[2S_i(kL_s) - S_i(2kL_s) - sin(kL_s)]\left[2C_i(kL_s) - C_i(2kL_s) - C_i\left(\frac{2kW^2}{L_s}\right)\right]\} \tag{3.7}$$

Where $S_i(x)$ and $C_i(x)$ are the sine and cosine integrals defined as,

$$S_i(x) = \int_0^x \frac{\sin(x)}{x} dx \tag{3.8}$$

$$C_i(x) = -\int_0^\infty \frac{\sin(x)}{x} dx \tag{3.9}$$

Table 3.1 Geometrical parameters of the proposed antenna

Parameter	Value (mm)	Parameter	Value (mm)
L	124	S1	34.641
W	124	S2	46.188
L_1	93	S3	57.735
L_2	94	R_{in}	0.47
a	38.5	W	8

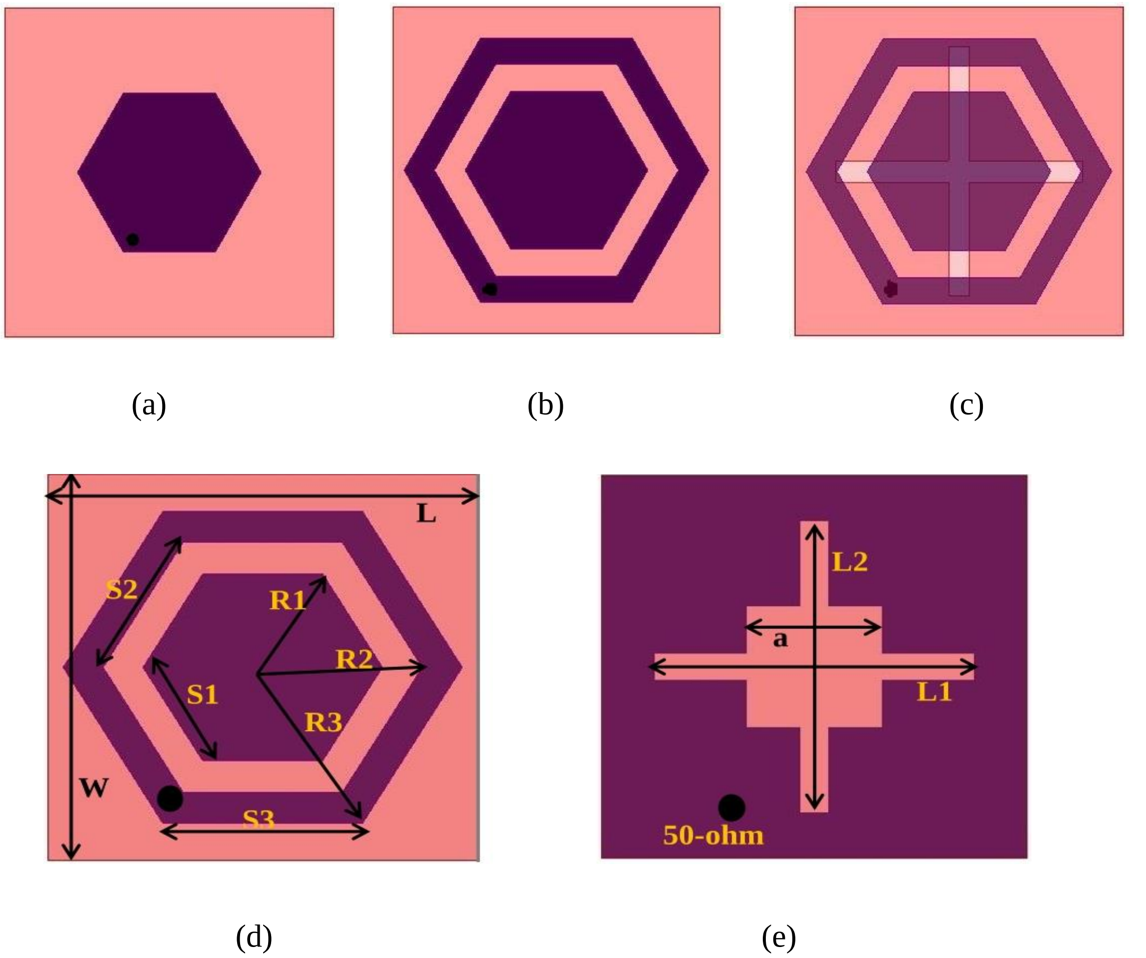

Figure 3.1 Evaluation of the proposed antenna (a) Antenna-1 (b) Antenna-2 (c) Antenna-3 (d) Proposed antenna top view (e) Proposed antenna bottom view

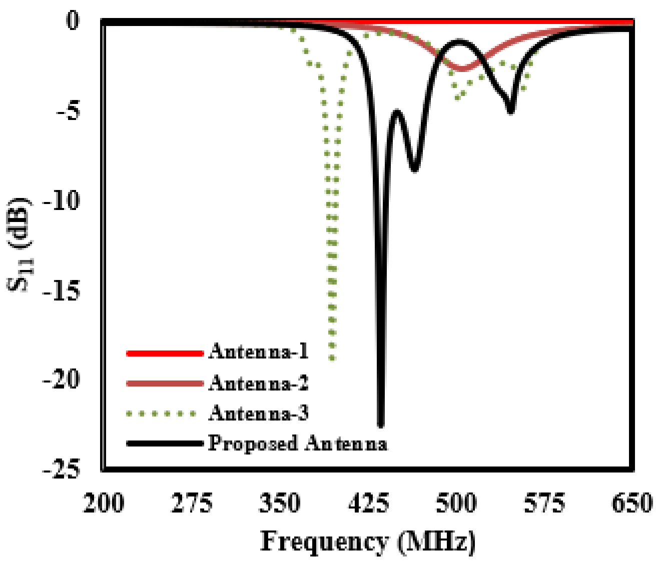

Figure 3.2 Step-wise simulated S_{11} results of the proposed antenna

(a) (b)

Figure 3.3 Fabricated antenna (a) Top view (b) Bottom view

3.1.3. Phantom Model

As per IEEE standard three-layered phantom tissue model with water. Water bolus layered has different significances for taking into consideration it makes the EM field transmission into the phantom with less reflection from the surface, it is also used for cooling down the skin layer at constant temperature and one more interesting function of water bolus layer is to protect the EM field radiation at a safety level. The relative permittivity of each layer is different. We have to make a single-layer phantom as per measurement availability in a laboratory. Effective permittivity for single layer phantom tissue model is given in equation (3.10).

$$\epsilon_{eff} = (\epsilon_{r1} + \epsilon_{r2})/2 \quad (3.10)$$

Where ϵ_{r1} and ϵ_{r2} are the relative permittivity of different layers, using the above equation calculate the effective permittivity of phantom tissue. The model overloads the antenna fields and provides the main SAR pattern due to the combined strength. Dielectric parameters, permittivity (ϵ_r) are 64.28, conductivity (σ) is 0.253 S/m, and density (ρ) is 1100 kg/m^3 in the ISM band [19, 110, 111]. The size of cubical phantoms is 190x130x50 mm^3 taking into consideration for simulation as well as during measurement. The height of the tissues layered was limited to 50 mm, due to relatively moderate losses, fat tissue does not significantly contribute to the averaged SAR [101]. To account for extra variations [110], we have varied the distance from 3cm to 9cm with a step size of 3cm between the antenna and phantom.

3.1.4. Results and Discussion

3.1.4.1. Reflection Coefficient

Figure 3.4 shows the comparison of simulated v/s measured reflection coefficient with and without Phantom. The simulated value of the reflection coefficient is -22.3 dB and the measured value of the reflection coefficient is -21.1 dB in the case of without phantom. In the case of the TEL phantom simulated and measured reflection coefficient at a 3cm distance between the phantom and antenna is 12.1 dB and -8.9 dB respectively. The differences between the simulated and measured results can be attributed to the manufacturing tolerances, quality of the SMA connector, and scattering environment. For reflection coefficient measurement shown in Figure 3.5, the antenna is directly connected to a spectrum analyzer (R&S FSH8 100 kHz-8 GHz) with a probe.

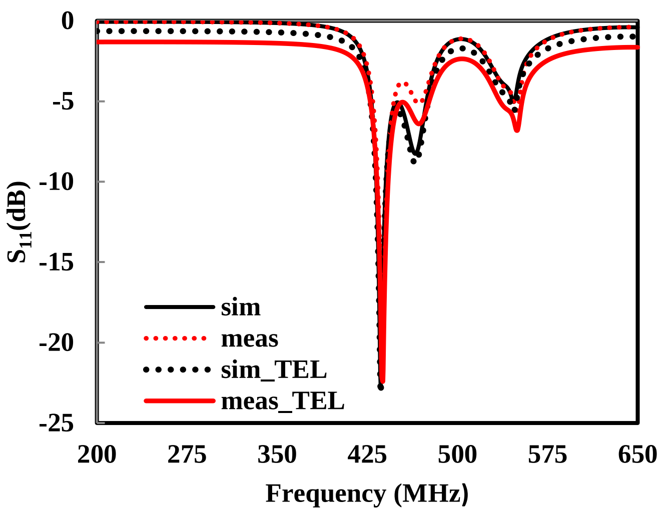

Figure 3.4 Simulated and measured S_{11} with TEL phantom and without phantom

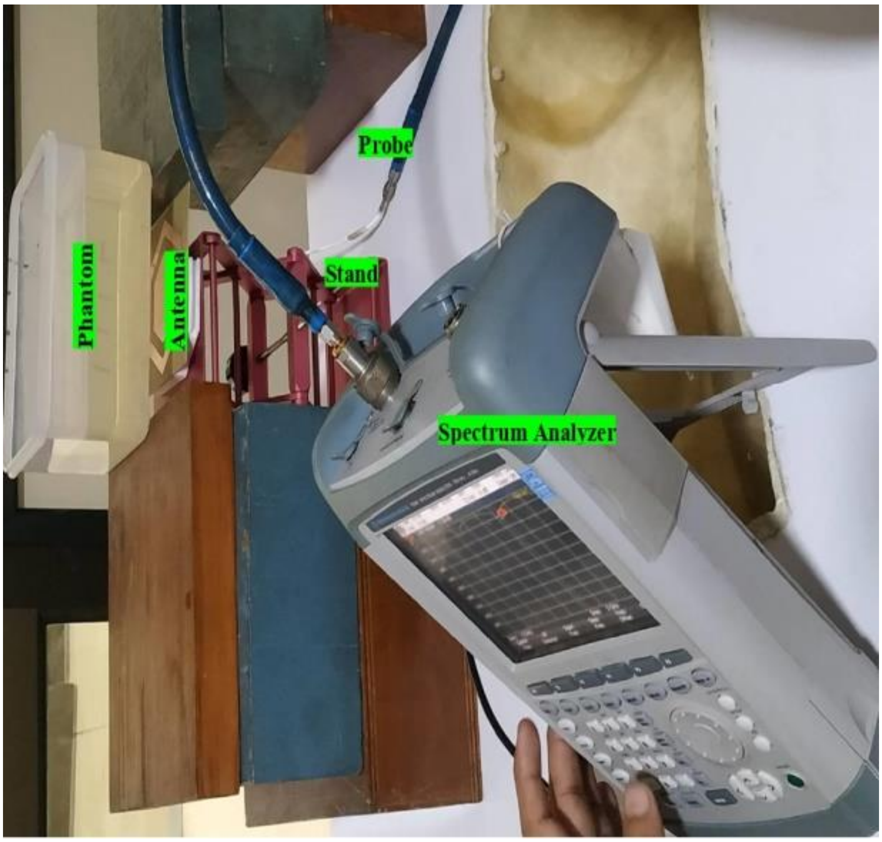

Figure 3.5 Measurement setup of S_{11}

3.1.4.2. Specific Absorption Rate (SAR)

The Specific absorption rate is a measure of the amount of power deposited by a radiofrequency field in a certain mass of tissue. Figure 3.6(a) shows the simulated SAR value of 0.4 W/kg along the x-axis at a 3cm phantom distance from the antenna. SAR is determined by measuring the Electric Field (E) inside the TEL Phantom shown in Figure 3.6(b). Fix the antenna and Phantom position at a 3cm distance. Set the Power level of the SMR signal generator (R&S SMB100A 10 MHz-40 GHz) is 0dBm i.e. 1 mw set the operating frequency is 434 MHz and connect with the probe to the antenna. Now set the same frequency in the spectrum analyzer and connect one port with the Electric Probe [106, 112] and another port to the computer. Now, the Electric Probe [106] is inserted into the TEL Phantom to different positions along the variation of the x-axis for Electric field reading, After getting the Electric field value, SAR will be calculated by equation (3.11) in terms of the Electric field, conductivity, and density of the tissue, results are summarized in Table 3.2.

$$SAR = \frac{\sigma E^2}{2\rho} \text{ (W/kg)} \quad (3.11)$$

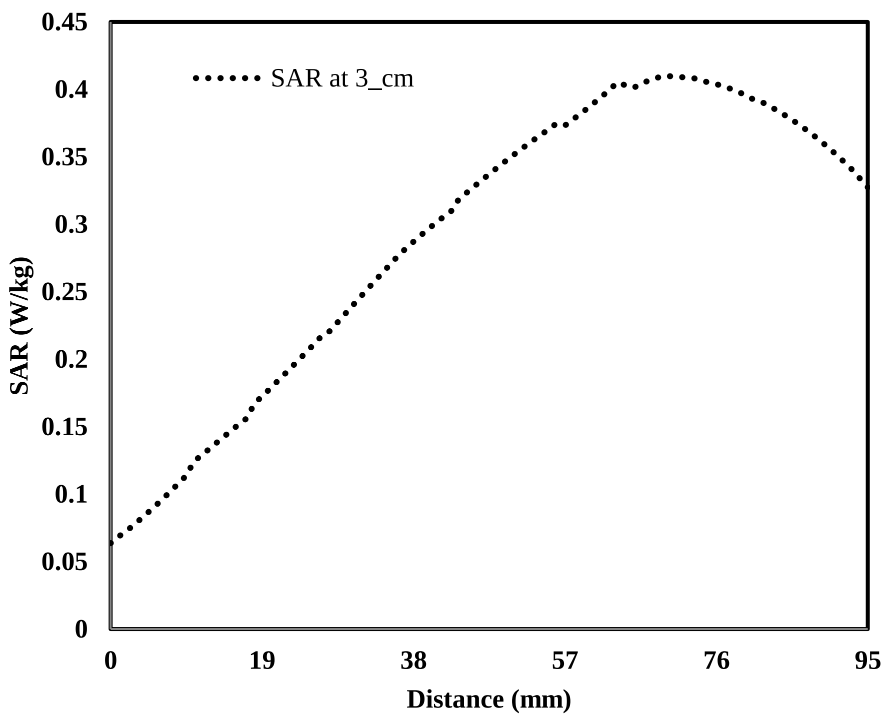

(a)

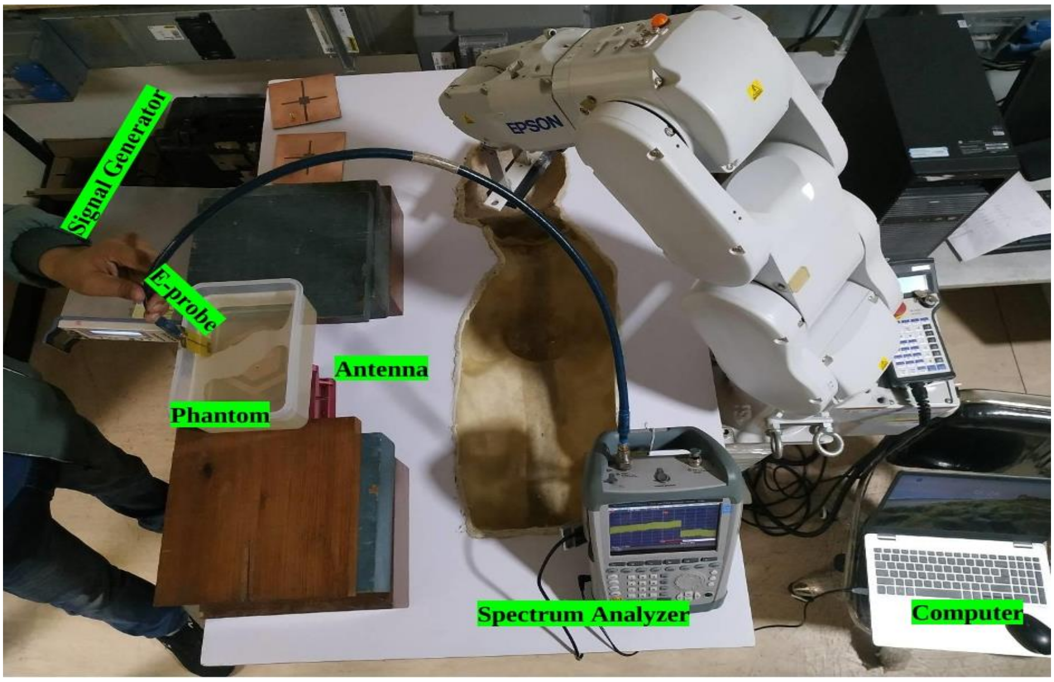

(b)

Figure 3.6 (a) Simulated SAR value along the x-axis at a 3cm distance between TEL phantom and antenna (b) Measurement of Electric field

Table 3.2 Calculated SAR value when the E- fields were measured along the x-axis

Phantom Detail	Distance b/w antenna and Phantom (d) in cm	Distance inside the Phantom (x_1) in cm	Measured E-Field at (x_1) V/m	SAR (W/kg)
TEL	3	5.0	44.75	0.2303
		6.5	45.26	0.2355
		8.0	45.89	0.2422
		9.5	46.57	0.2494

3.1.4.3. Radiation Pattern

The illustration in the Figure 3.7 below depicts the simulated radiation pattern characteristics at 434 MHz for the proposed antenna structure. Analysis of the E-plane characteristic reveals a distinctive dipole-like behavior. This behavior is consistent with the expected radiation pattern of a dipole antenna, where radiation is predominantly observed along the plane perpendicular to the antenna's axis. The presence of two lobes, each with a peak intensity, signifies the constructive interference resulting from the phased emission of electromagnetic waves. Contrastingly, the H-plane characteristic illustrates an omnidirectional radiation pattern, indicative of equal radiation intensity in all azimuthal directions. This is a desirable trait for applications necessitating uniform coverage in the horizontal plane. The maximum achievable gain is -9.2 dB.

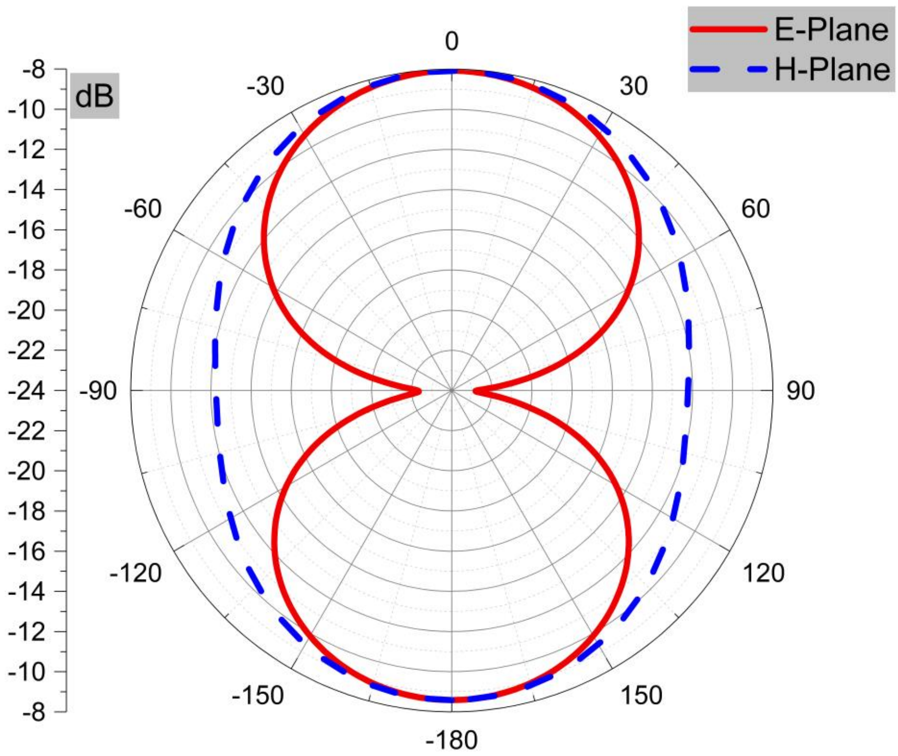

Figure 3.7 Radiation Pattern of the proposed hexagonal antenna structure

Table 3.3 Qualitative Comparison of reported antennas to the proposed antenna

Ref.	Freq.	S_{11}(dB)	SAR(W/kg)	Size(mm)	Application
[19]	434 MHz	-13.8	1.32	130×130 ×2.97	MICS
[56]	434 MHz 915 MHz	-16 -17	1.32 1.44	124×124 ×1.6	MICS
[113]	915 MHz 2.45 GHz	-32 -27	11.17 27.93	120×120×2.007	MICS ISM
This work	434 MHz	-22.3	0.4	124×124 ×1.6	MICS

From Table 3.3 it can be concluded that the proposed antenna operates at 434 MHz with a reflection coefficient of -22.3 dB and shows a better SAR value of 0.4 W/kg than the antenna structures reported in [19, 56, 113].

3.1.5. Summary

In this work, a hexagonal patch antenna was designed at 434 MHz for hyperthermia application. The antenna performance is compared at different distances from the phantom model using FEM modelling. SAR and reflection coefficient have been evaluated at a 3 cm distance from the phantom. The value of SAR lies in the permissible limit of the exposed body as stated by IEEE standards. To be precise the SAR designed a differently shaped structure at the same band and check the SAR performance with different distances in upcoming section 3.2 of this chapter.

3.2. Slot-Loaded Pentagon Microstrip Patch Antenna for Hyperthermia Applications at 434 MHz

3.2.1. Introduction

It has been found that limited of the published articles has investigated their respective research with a variety of distances between antenna and phantom for the treatment of hyperthermia. To bridge this research, gap the novelty of the proposed antenna is to operate in the ISM band with and obtain the comparable value of SAR with the phantom tissue materials. The rest of the chapter is organized as follows: Section 3 provides a detailed description of a slotted pentagon-shaped microstrip patch antenna and TEL phantom tissue model. Section 4 presents the experimental results, including S_{11}, surface current, thermal analysis, radiation pattern, and SAR, the maximum power to be delivered to the antenna was calculated in accordance with the SAR limitation after simulating to assure antenna safety. Section 5 covered the measurement procedure. The performance of an antenna prototype was compared before the conclusion section.

3.2.2. Antenna Design

In this part, FR-4 copper laminated dielectric substrate of dimension 120x120x1.6 mm^3 having a dielectric constant of 4.4, and a loss tangent (tanδ) of 0.02 is used. The size of the pentagon is determined by equation (3.12). The proposed antenna design starts from the basic pentagon patch of size S_1=39.95 mm as shown in Fig. 3.6, then introduces a pentagonal annular ring of size S_2= 49.35 mm and, S_3= 58.75 mm as shown in Fig. 3.7. Then introduce slots on the ground plane shown in Fig. 3.6 having different lengths and the same width ground plane that improves the reflection coefficient but degrades the bandwidth, and finally introduce a square slot having side (a) which is positioned exactly behind the pentagon patch. Slots in the ground plane change the resonant currents path on the pentagon patch as well as on the annular ring to reduce the overall patch dimensions and also act like a load that can be used to bring the input impedance point closer to the characteristic impedance when added to the antenna. The Final proposed antenna configuration is illustrated in Fig. 3.8. The geometrical parameters of the proposed structure are shown in Table 3.4. 50-ohm coaxial feed is applied at the annular ring with an inner radius of 0.47mm. For the initial design of the antenna, take relations regarding the rectangular patches and their corresponding transmission line models. A Single-layered biological tissue TEL model was taken throughout the design procedure and simulation of the antenna. Where S is the size of the pentagon, r is the radius, and O is the center of the inscribed circle of the pentagon.

$$S=1.175r \tag{3.12}$$

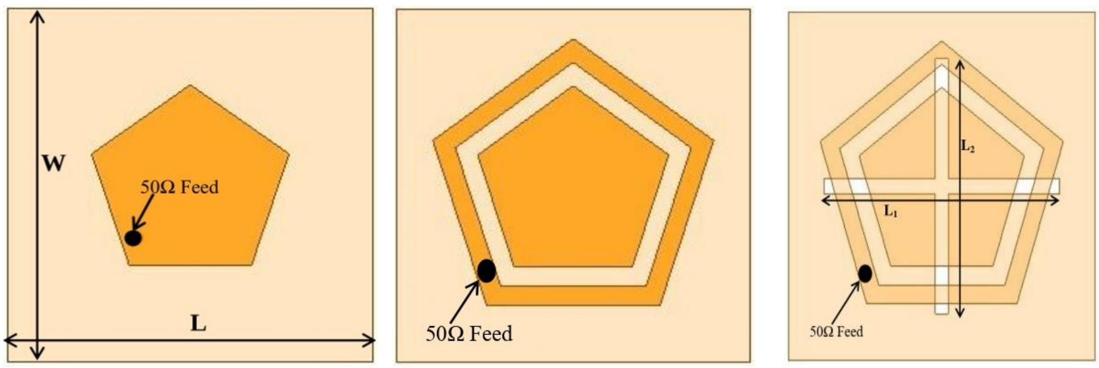

(a) Step-1 (b) Step-2 (c) Step-3

Figure 3.8 Step-by-step design of the proposed antenna

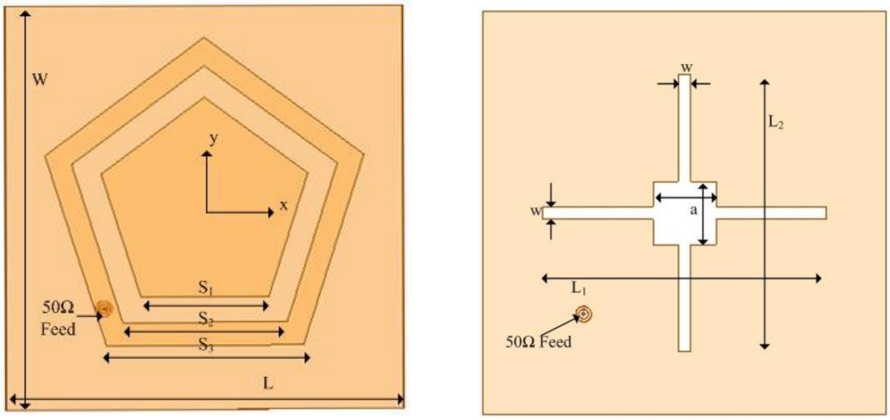

(a) Top view (b) Bottom view

Figure 3.9 The geometrical configuration of the proposed antenna.

Table 3.4 Geometrical parameters of the proposed antenna

Parameter	Value (mm)	Parameter	Value (mm)
L	120	r_1	34
W	120	r_2	42
L_1	88	r_3	50
L_2	86	R_{in}	0.47
A	18	W	5

3.2.3. Phantom Model

A planar single-layered tissue model TEL phantom was used to analyze the performance of SAR at different distances from the antenna. Water bolus layered has different significances for taking into consideration it makes the EM field transmission into the phantom with less reflection from the surface, it is also used for cooling down the skin layer at constant temperature and one more interesting function of water bolus layer is to protect the EM field radiation at a safety level. Parameters of heterogeneous body tissues are described in [114] and the underline geometries with detailed descriptions of the phantom body tissue are available for in-silico analysis [110]. To reduce computational resources and for clarity, a single-layered tissue model was used. The model overloads the antenna fields and provides the main SAR pattern due to the combined strength. The dielectric properties of the phantom are permittivity (ϵ_r) is

64.28, conductivity (σ) is 0.253 S/m, and density (ρ) is 1100 kg/m^3 [110, 111, 113, 115] for 434 MHz. The size of cubical phantoms is 190x130x50 mm^3 taking into consideration for simulation as well as during measurement. The height of the tissue layer was limited to 50 mm, due to relatively moderate losses, fat tissue does not significantly contribute to the averaged SAR [101, 116-118].

To account for extra variations, varied the distance from 3cm to 9cm with a step size of 3cm between the antenna and phantom.

3.2.4. Results and Discussion

3.2.4.1. Reflection Coefficient

Fig.3.9 shows the reflection coefficient comparison of each step. Fig.3.10 shows the value of simulated and measured reflection coefficients without Phantom which are very close to each other, the simulated value of the reflection coefficient is -15.19 dB and the measured value of the reflection coefficient is -31.53 dB. Fig.3.11 shows the value of the simulated and measured reflection coefficient with the TEL phantom. Simulated and measured reflection coefficient values are -21.23 dB and -26.42 dB respectively.

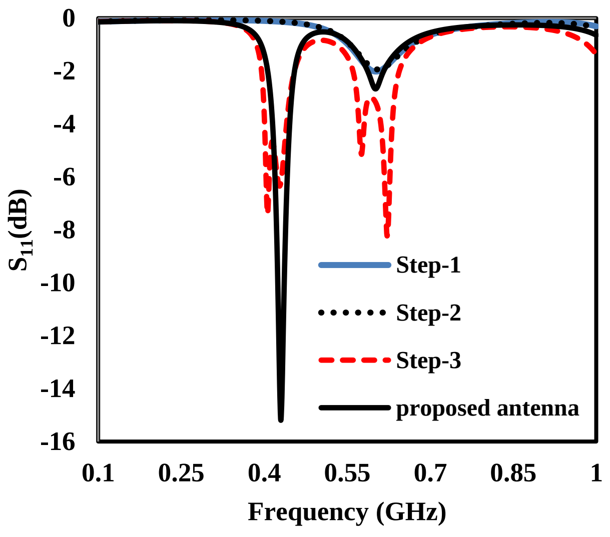

Figure 3.10 Simulated results of all steps without phantom (free space)

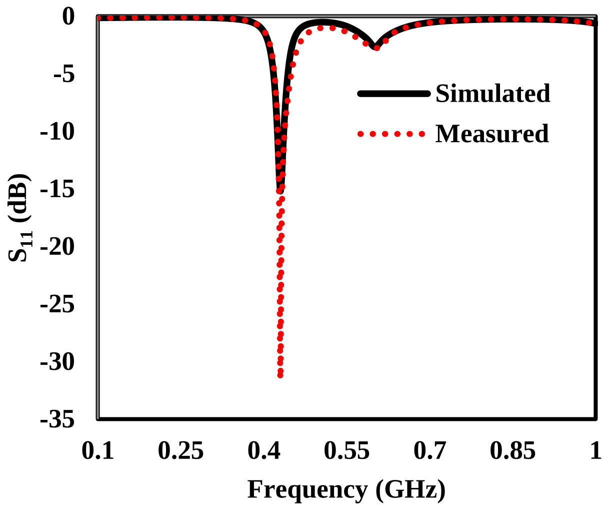

Figure 3.11 Simulated and measured S_{11} of the antenna without phantom (free space)

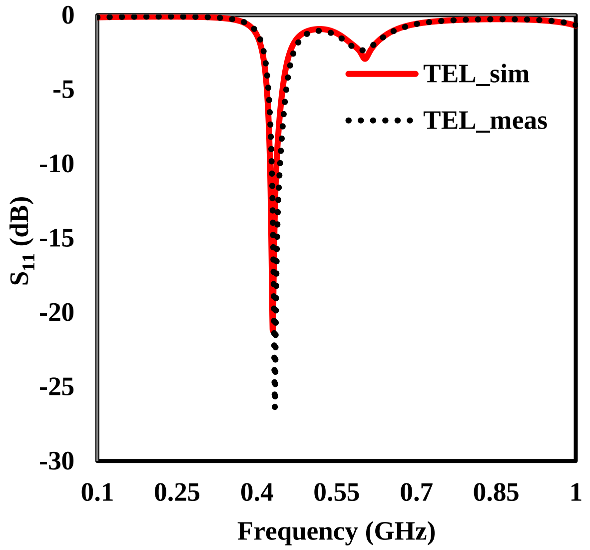

Figure 3.12 Simulated and measured S_{11} with TEL Phantom

3.2.4.2. Surface Current

A small defect on the ground plane under the patch should perturb the exited EM fields. This, in turn, should cause several changes in the field profile orientation of the patch antenna. This basic idea has been implemented to improve the antenna characteristics. The orthogonal slot combined with a square slot on the bottom side, shown in Fig. 3.14, where ground-defected surfaces are strategically located on the H-plane of the antenna. The designed frequency is adjusted by coupling resonant currents on the circumferences of the pentagon patch as well as the pentagonal ring. The analysis of current distributions at the top with and without a slot and bottom with and without a slot part is used to obtain the elaborated electromagnetic conduction of the proposed antenna, as shown in Fig. 3.12-3.15, it is observed that the orientation of the current is concentrated to feed and the boundaries of the pentagonal annular ring, thus excited mode was TM_{11}. It is observed that the strong current is distributed at the top and bottom in the case of the slot. However, the highly concentrated vector current in each case is orthogonal to each other and accommodates one-half wavelength corresponding to the resonating frequency.

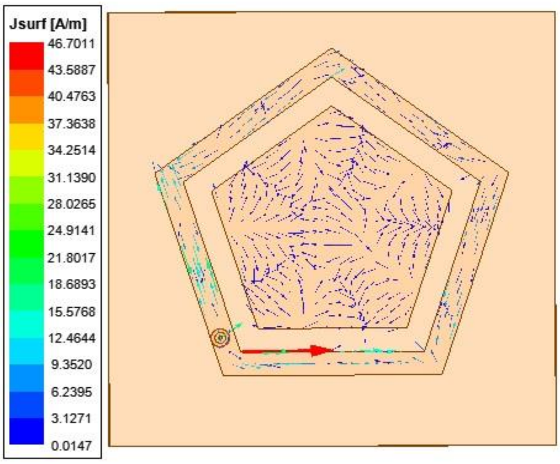

Figure 3.13 Current distribution on top without slot

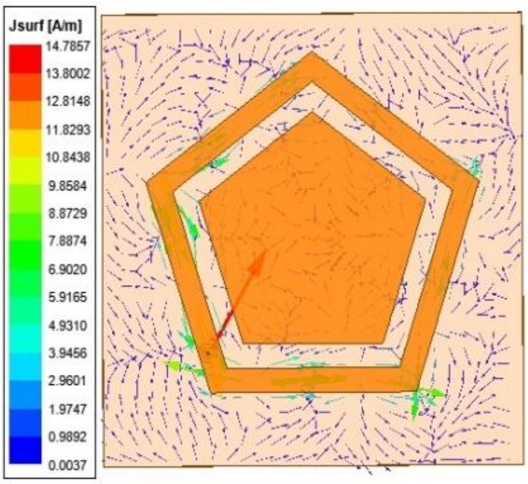

Figure 3.14 Current distribution on the bottom without slot

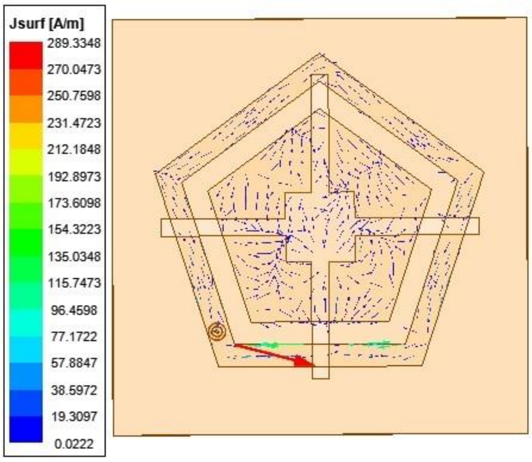

Figure 3.15 Current distribution on top with slot

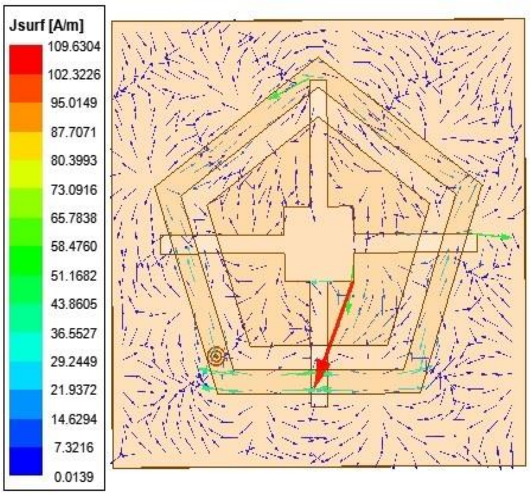

Figure 3.16 Current distribution on the bottom with slot

3.2.4.3. Specific Absorption Rate (SAR)

The Specific absorption rate is the measurement of the rate at which energy is absorbed per unit mass by a human body when exposed to a radio frequency (RF) electromagnetic field. It is calculated by using the formula given in equation (3.11). It is determined by measuring the Electric Field (E) inside the different tissue Phantom materials at different penetration depths. Fix the antenna and Phantom at a 3cm distance. Then measured Electric Field along the x-axis at 5cm, 6.5cm, 8cm, and 9.5cm inside the Phantoms, the results are summarized in Table 3.5.

In the simulation, three different cases were considered for SAR calculation. Fig.3.16 shows the SAR value along the x-axis penetration depth when the phantom is placed at 3cm, 6cm, and 9cm distances from the antenna respectively.

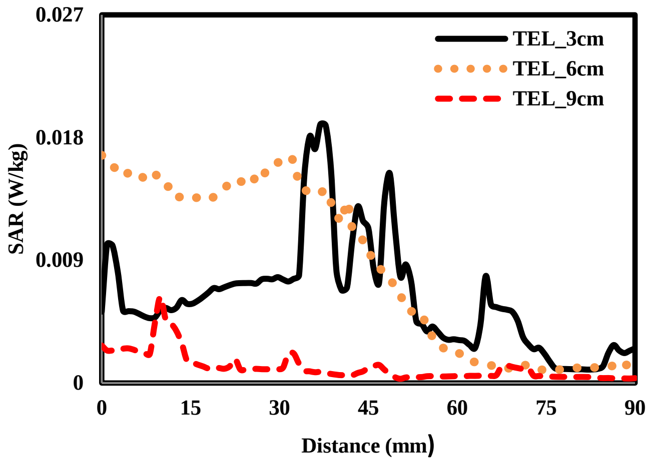

Figure 3.17 Simulated SAR value along the x-axis at 3 cm, 6 cm, and 9 cm.

From Table 3.5, it can be concluded that SAR is the nonlinear function of distance. As can be seen, the SAR value is 0.089 W/kg when the E-field is measured along the x-axis inside the phantom at 5 cm penetration depth inside the TEL phantom.

Table 3.5 SAR calculation when the E- fields were measured along the x-axis

Phantom Details	Distance b/w antenna and Phantom (d) in cm	Distance inside the Phantom (x_1) in cm	Measured E-Field at (x_1) V/m	SAR (W/kg)
TEL	3	5.0	5.63	0.089
		6.5	5.99	0.101
		8.0	4.93	0.068
		9.5	4.65	0.061

3.2.4.4. Radiation Pattern

Simulated radiation plots of the proposed antenna for E-plane and H-Plane at 434 MHz are shown in Fig.3.16. The maximum simulated gain obtained at 434 MHz is -9.1 dBi. From Fig.3.17 it is observed that the radiation patterns are bidirectional to the surface, which is desirable for biomedical applications.

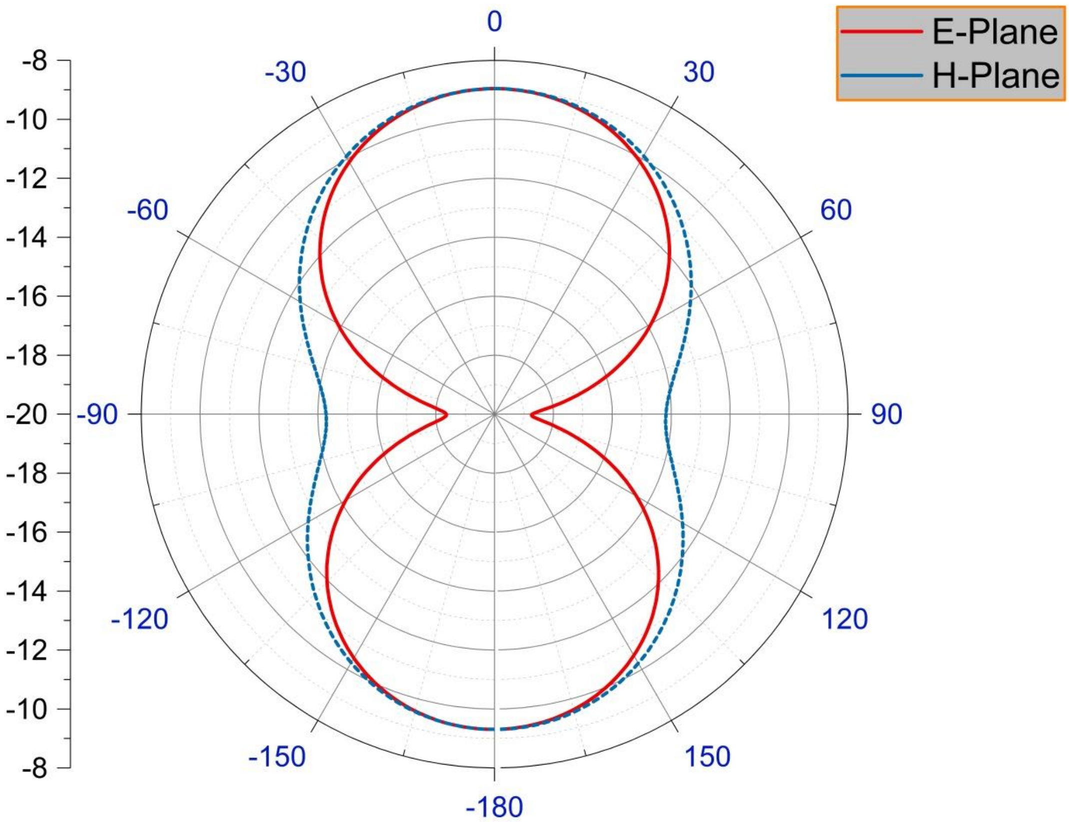

Figure 3.18 Simulated radiation pattern plot

3.2.4.5. Fabrication and Measurement

Fig.3.18(a) and Fig. 3.18(b) show the fabricated prototype of the proposed antenna top and bottom view respectively.

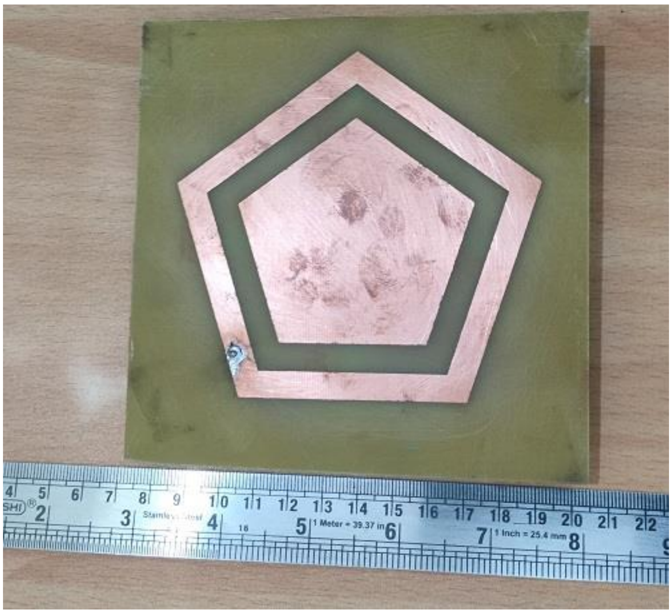

(a)

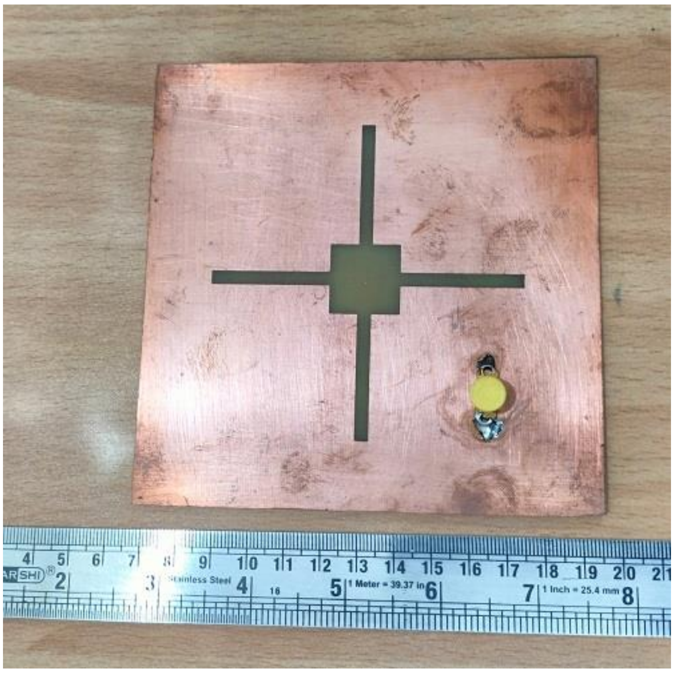

(b)

Figure 3.19 Fabricated prototype of the antenna (a) Top view (b) Bottom view

Fig. 3.19(a) and Fig. 3.19(b) show the measurement of the reflection coefficient and Electric field measurement respectively. For reflection coefficient measurement, the antenna is directly connected to the spectrum analyzer (R&S FSH8 100kHz-8GHz) with the probe.

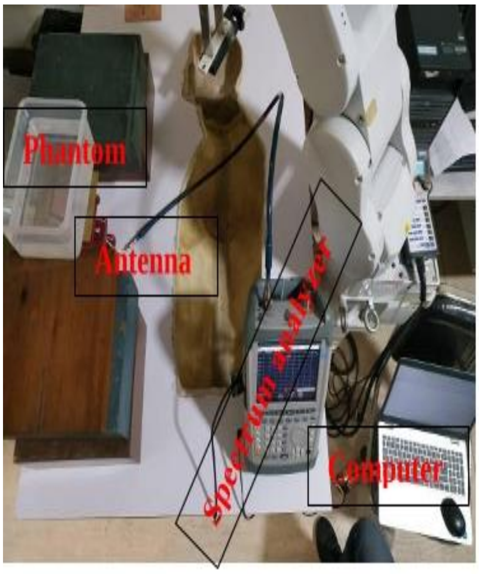

(a)

(b)

Figure 3.20 Measurement of pentagon patch antenna (a) S_{11} (b) E-field

Table 3.6 Qualitative comparison of reported antennas to the proposed antenna

Ref.	Freq	S_{11} (dB)	SAR (W/kg)	Size(mm^3)	App.
[19]	434 MHz	-13.8	1.32	130×130 ×2.97	MICS
[56]	434 MHz	-16	1.32	124×124 ×1.6	MICS ISM
	915 MHz	-17	1.44		
[113]	915 MHz	-32	11.17	120×120×2.007	ISM
	2.45 GHz	-27	27.93		
This work	434 MHz	-15.19	0.089	120×120 ×1.6	MICS

From Table 3.6, it can be concluded that the proposed antenna operates in the ISM band and shows a better SAR value as per IEEE standard comparison to other structures reported in [19, 56, 113].

3.2.5. Summary

In this work, a pentagon patch antenna for hyperthermia application has been designed. A microstrip patch antenna is less complex to fabricate as compared to the waveguide and horn antenna. The slotted technique on the ground surface is used for impedance matching. The antenna performance is compared at different distances from the phantom model using FEM modelling. SAR and reflection coefficient have been evaluated with phantom models. Simulated and measured results are very close to each other. From the above analysis, it has been observed that the value of SAR has a non-linear relationship with distance. The value of SAR lies in the permissible limit of the exposed bodies as stated by IEEE standards.

3.2.6. Conclusion

In essence, a hexagonal and a pentagonal patch antenna were designed at 434 MHz for hyperthermia applications. Both antennas were fabricated and measured in free space as well as in phantom. Furthermore, SAR evaluation at different distance were measured.

The transition from the MICS band to the ISM band will be addressed in the upcoming Chapter 4.